Journal of Global Environment Engineering, Vol. 7, pp. 79-99, 2001

NUMERICAL SIMULATION OF THE TRANSPORT OF BIOMASS BURNING EMISSIONS IN SOUTHEAST ASIA - SEPTEMBER AND OCTOBER, 1994 -

Toshihiro Kitada[1]
Masato Nishizawa[2]
Gakuji Kurata[3]
Yutaka Kondo[4]

Abstract

Biomass burning in tropical Southeast Asia was examined with the numerical simulation of a transport/chemistry/deposition model. Effect of the biomass burning (fire) emissions on ozone and CO concentrations was quantified over equatorial Asia, i.e. the Malay Peninsula, Indonesia, and northern Australia. Ozone vertical soundings at two meteorologically-different sites, i.e., Kuala Lumpur under active vertical mixing, and Watukosek, Java, in stably stratified condition, were used for model validation. How far the biomass fire influences was quantified, and during these simulations importance of initial plume rise due to biomass fire in stable condition was stressed. Biomass burning sources contributed to the total increase of ozone column density, which was chemically produced from all the emission sources, by 35 % in the southern Malay Peninsula, 60% in eastern Java, and 70% in northern Australia.

KEYWORDS: biomass burning, southeast Asia, air pollution modeling, ozone, carbon monoxide

1. Introduction

Biomass burning is now widely recognized as one of the most important emission sources of trace chemical species in global scale (e.g., Crutzen and Andrea, 1990). Its effect extends from global warming through green house gas emissions to local air pollution. Southeast Asia is one of the major areas of biomass burning in the world. In fact, in the dry season of 1993, 1994 and 1997, severe biomass burning occurred in tropical Southeast Asia, i.e. the islands of Sumatra and Borneo, Indonesia, and it resulted in various types of air pollution over large area by emitting aerosol particles and photochemical precursors (Matsueda, et al. 1998; Tsutsumi, et al. 1999). That event is caused by mixed reasons of human activity and natural conditions, and occurs periodically every two or three

[1] Dr. Eng. Prof., Dep. Ecological Eng., Toyohashi Univ. of Technology, Toyohashi 441-8580, JAPAN
[2] Dr. Eng. Japan Atomic Energy Research Institute, Tokai-mura, Ibaraki 319-1195, JAPAN
[3] Dr. Eng. Res. Assoc., Dep. Ecological Eng., Toyohashi Univ. of Technology, Toyohashi, JAPAN
[4] Dr. Sci. Prof., RCAST, The University of Tokyo, Komaba, Meguro-ku, Tokyo 153-8904, JAPAN

years in the dry season enhanced by "El Niño and Southern Oscillation (ENSO)". Thus we have evaluated effects of the biomass burning on the concentration fields of trace chemical species and on the tropospheric chemistry in East and Southeast Asia scale in September and October, 1994, by applying our transport/chemistry model described in Kitada and Nishizawa (1998) and Kitada et al. (1998), and trajectory calculation. Several modeling studies, which investigate impacts of biomass burning on several key chemical species in the Southeast Asia, have been performed. For example, Galanter et al. (2000), Wang et al. (1998), etc. used global scale modeling. As described above, we focused on regional scale or semi-global scale problem for tropical Southeast Asia. The calculation included anthropogenic emissions of various chemical species, and NOx emissions from lightning and soil microbial activity. On biomass burning, EDGAR annual emission was modified by considering distribution of fire activity archived by IGBP-DIS Global Fire Product. The biomass burning in northern Australia, which was not included in EDGAR, was estimated in this study.

Obtained results were compared with vertical soundings of ozone at Kuala Lumpur (KL) in Malaysia and Watukosek (WK) in Java, Indonesia, as well as with surface ozone observation at Singapore. Transport characteristics in tropical Southeast Asia was also discussed in connection with the vertical profiles of ozone mixing ratio. Furthermore, contribution of the biomass burning to the concentrations of several key chemical species was evaluated.

2. TRANSPORT/CHEMISTRY/DEPOSITION MODEL FOR TRACE CHEMICAL SPECIES AND EMISSION SOURCES

2.1 Summary of the Model

Equations for transport/chemistry/deposition (Kitada and Nishizawa, 1998; Kitada et al. 1998) were numerically integrated from 00GMT on 15 September to 00 GMT on 5 October, 1994. The domain was 80°E - 160°E, 19°S - 60°N, and the earth's surface - 10hPa. Grid size was 1° in horizontal directions, and variable 17 layers were used in vertical direction. The model includes processes of advection, diffusion, sub-grid scale cumulus convection, chemical reactions, and wet and dry depositions. Chemical species treated in the model were 38, 25 of which were advected. These species were tied with a system of 90 chemical reactions; the reaction system was an adaptation from Lurmann et al. (1986) with some of the updated reaction rate constants listed in NASA Panel for Data Evaluation (1997). ECMWF operational analysis data were used for wind, temperature, and water vapor etc. and they were renewed every 6 hours. These data were interpolated every time step, i.e. 30 minutes, for simulation. Precipitation was provided every 24 hours. The applied governing equations are as follows, where a spherical coordinate with σ transformation for vertical direction is used:

$$C\frac{\partial X_i}{\partial t} + Cv_\phi \frac{\partial X_i}{\partial x} + Cv_\theta \frac{\partial X_i}{\partial y} + C\dot{\sigma}\frac{\partial X_i}{\partial \sigma} = \frac{\partial}{\partial x}\left(CE_\phi \frac{\partial X_i}{\partial x}\right) + \frac{1}{\cos\theta}\frac{\partial}{\partial y}\left(C\cos\theta \cdot E_\theta \frac{\partial X_i}{\partial y}\right)$$
$$+ \frac{\rho g^2}{r^2\pi^2}\frac{\partial}{\partial \sigma}\left(C\rho r^2 E_\sigma \frac{\partial X_i}{\partial \sigma}\right) + R_i + W_i + Q_{V,i} \qquad i = 1, 2, \cdots, 38 \qquad (1)$$

where X_i denotes dimensionless concentration of the "i" th chemical species, C (kmol/m^3) and

ρ (kg/m^3) stand for air density, $dx \equiv r\cos\theta \cdot d\phi$, $dy \equiv rd\theta$, $\sigma \equiv (p - p_T)/\pi$, $\pi \equiv p_S - p_T$, $p_S, and\ p_T$ the atmospheric pressure at surface and top boundaries, respectively, $\dot{\sigma} \equiv \rho g\{(\partial z/\partial t)_\sigma + \vec{v}\cdot\nabla_\sigma z - v_r\}/\pi$, $E_\phi, E_\theta, and\ E_\sigma$ (m^2/s) eddy diffusivities for $\phi, \theta, and\ \sigma$, respectively, r the distance from the earth's center (m), z the distance from mean sea level to the height of a "σ" value (m), R_i the chemical reaction rate (kmol/m^{3}s), W_i the wet deposition rate (kmol/m^{3}s) (see Kitada and Nishizawa, 1998 for the detail of W_i), and $Q_{V,i}$ the volume-emission source (kmol/m^{3}s). The equation system (1) is solved using a finite element method with a semi-analytic solver for chemistry part. On the vertical boundary conditions, constant concentrations of climatic values are given at the upper boundary of 10 hPa, and at the surface boundary, the following equation is applied,

$$CE_\sigma \frac{\rho g}{\pi}\frac{\partial X_i}{\partial \sigma} = Q_{S,i} - v_{g,i}CX_i \tag{2}$$

where $Q_{S,i}$ the emission source strength at surface level (kmol/m^{2}s), and $v_{g,i}$ the deposition velocity (m/s). On the lateral boundary conditions, the following approximated equations are used, for example, at the west boundary,

for in-flow case, i.e., $v_\phi \geq 0$,

$$v_\phi CX_i - CE_\phi \frac{\partial X_i}{\partial x} = v_\phi CX_{B,i} \tag{3}$$

for out-flow case, i.e., $v_\phi < 0$,

$$\frac{\partial X_i}{\partial x} = 0 \tag{4}$$

where $X_{B,i}$ denotes concentration at outside of the boundary, and is given with the concentration on the boundary at the previous time step except for the case in which always $v_\phi \geq 0$ after the start of simulation, i.e., initial concentration is used as $X_{B,i}$ in this case. Initial concentrations were assumed by using climatic values. Since Eqs. (3) and (4) are incorporated into calculations through the "natural" boundary condition in a finite element formulation, the boundary condition of Eq. (4) does not mean "perfect reflection" but does "flow through" with advection term.

Application of a sub-grid cumulus convection scheme was judged by examining both vertical profile of relative humidity and upward wind at about a height of 1 km above ground. Cloud mass flux from atmospheric boundary layer (ABL) into free troposphere due to the cumulus convection was determined with the vertical wind velocity at about 1 km high, and the air mass subtracted from ABL was vertically distributed. This cumulus convection scheme is conceptually similar to that in Strand and Hov (1993). The activity map of cumulus convection will be shown later in Fig. 2, which was estimated in this study from 1°x 1° ECMWF meteorological data. The procedure is as follows: (1) check vertical profile of relative humidity, and find the place at which it exceeds 80% at the top of

the air column and is kept to be over 60% through the air column down to the surface level; moreover, (2) when the vertical wind at the top of the boundary layer (BL) is upward, then the cumulus convection scheme is applied; and, (3) cloud mass flux at the top of BL is determined with the vertical wind velocity in resolvable scale.

2.2 Emission Sources Including Biomass Fire

Various types of emission sources were considered in this study. Those of NO_X, for example, are

Table 1. NOx and CO emissions in calculation domain,

(a) NOx in whole area:80E～160E and 19S～60N(AUSMIN2)

Source type		Strength(kgN/mon)	Relative Strength	Reference
Fossil fuel		3.78×10^{8}	0.554	EDGAR(1997)
Biomass Burning	Biofuel	6.48×10^{7}	0.095	EDGAR(1997)
	Biomass fire	$(1.76+0.57^{*})\times10^{7}$	0.034	EDGAR & this study
	Waste	5.80×10^{7}	0.085	EDGAR(1997)
Soil		5.95×10^{7}	0.087	Yienger and Levy(1995)
Lightning		4.19×10^{7}	0.061	Based on Kumar et al.(1995)
Aircraft		5.40×10^{6}	0.008	NASA LaRC(1999)
Total		6.82×10^{8}	1	

*Biomass burning source in Australia (this study).

(b) NOx in limited tropical area: 90E～120E and 10S～10N

Source type		Strength(kgN/mon)	Relative Strength	Reference
Fossil fuel		2.05×10^{7}	0.313	EDGAR(1997)
Biomass Burning	Biofuel	0.68×10^{7}	0.104	EDGAR(1997)
	Biomass fire	1.16×10^{7}	0.177	EDGAR & this study
	Waste	0.55×10^{7}	0.084	EDGAR(1997)
Soil		1.17×10^{7}	0.179	Yienger and Levy(1995)
Lightning		0.88×10^{7}	0.134	Kumar et al.(1995)
Aircraft		0.06×10^{7}	0.009	NASA LaRC(1999)
Total		6.55×10^{7}	1	

(c) CO in limited tropical area: 90E～120E and 10S～10N

Source type		Strength(kgC/mon)	Relative Strength	Reference
Fossil fuel		1.39×10^{8}	0.128	EDGAR(1997)
Biomass Burning	Biofuel	5.03×10^{8}	0.462	EDGAR(1997)
	Biomass fire	2.26×10^{8}	0.208	EDGAR & this study
	Waste	2.20×10^{8}	0.202	EDGAR(1997)
Aircraft		4.18×10^{5}	3.8×10^{-4}	NASA LaRC(1999)
Total		1.09×10^{9}	1	

listed in Table 1a,b, and CO in Table 1c. (As shown in Table1, EDGAR (1997) was a main data source, and emission sources for other chemical species such as hydrocarbons were also taken mainly from EDGAR except for biomass fire source in northern Australia). Since biomass fire activity shows strong seasonal variability and EDGAR gives annual emission, the biomass fire source of EDGAR was modified so that it is matched with those for September and October; fire activities archived in IGBP-DIS Global Fire Product (1999) were used for the modification.

In addition, since the biomass burning emission in Australia was not compiled in EDGAR, we estimated it with the IGBP-DIS Global Fire Product (1999), a vegetation map by NASA Goddard DAAC (1999), and the emission factors as described below.

The burned biomass, M (kg/grid cell), was estimated by $M = \sum_i (A * B * CF)_i$, where A denotes burned area in ha/grid cell, B the biomass density in kg/ha, CF the combustion factor (ratio of the burned biomass to existing biomass), and "i" the vegetation type. The burned area A was estimated using IGBP-DIS Global Fire Product. The factor B was also evaluated with vegetation map by NASA Goddard DAAC(1999) and biomass density information in Hao et al. (1990). We have assumed the following relation between combustion factor CF and monthly precipitation P (mm):

$CF_{forest} = 0.4 - 4.2^{-4} \times P$, and $CF_{grass} = 1 - 7.7^{-4} \times P$ for forest and grass land respectively. In these equations information on CF in Hao et al. (1990), Ward et al.(1992), Cautenet et al. (1999) etc. is taken into account. For example, when using this relation in the western part of the Middle Sumatra where monthly precipitation reached 500 mm in September, 1994, $CF_{forest} = 0.2$ can be obtained. Finally, emissions of chemical species from the burned biomass M were calculated with an equation $M_j = \sum_i (EF_j \times MC)_i$ where M_j denotes emission strength of the j-th chemical species in kg/kg-fuel-C, MC the carbon content in the burned biomass M (the ratio in weight was assumed 0.45 as in Ferek et al. 1998), and EF_j the emission factor for the "j" th species; the values in Ferek et al.(1998) were employed for EFj.

Relative importance of the biomass fire in the total NOx and CO emissions is shown in Table 1. In the whole calculation domain of East Asia (Table 1a), fossil fuel most contributes to the NO_X emission by 55%, and biomass fire accounts for only 3.4%. However, if we focus on Southeast Asia, the biomass fire can be one of the dominant emission source of NO_X and other chemical species. It explains about 18% of the NOx emission and exceeds 1/2 of the fossil fuel's (Table 1b), and also accounts for about 21% of the CO emission (Table 1c). Incidentally, the largest contributor to the CO emission is biofuel and is about 46%, suggesting together with low NOx emission from biofuel (Table 1b) that the biofuel is an important energy source in this area and its incomplete combustion due to low combustion temperature results in this characteristic emission pattern.

3. SIMULATION CASES

Table 2 lists simulation cases. BASE2 includes all the emission sources, but its biomass burning

source is that compiled in EDGAR and does not cover Australia. The cases of AUSMIN, AUSMIN2, and AUSMIN2R include Australian biomass burning. Although biomass burning is expressed with a

Table 2. Simulation cases

	All the sources except biomass burning	Biomass burning (EDGAR)	Biomass burning (Australia)
BASE2	○	○	
AUSMIN	○	○	○ (Flux type*)
AUSMIN2	○	○	○ (Volume type#)
AUSMIN2R (Standard)	○	○(Volume type$)	○ (Volume type#)
NOBB	○		
NOEMI			

* Emission source was expressed with a flux form at the earth's surface.
# The emission was given by uniform volume source from the surface to about 2.5km. Initial plume rise associated with biomass burning was assumed.
$ Biomass burning emissions in Java island, a part of New Guinea, etc. were given by a volume source (see Fig. 2).

flux form at the earth surface in most of the cases, two cases adopt a "volume" source for the emission from biomass burning, i.e., AUSMIN2R for Australia and the islands of Java etc. , Indonesia, and AUSMIN2 for Australia; see Fig. 2 for the area where the "volume" source was applied, i.e., the area enclosed with thick solid line. The "volume" source was used to see the effect of initial plume rise by sub-grid scale fire activity on the global scale chemical transport; it was applied for regions where strong high pressure system dominates and thus clear weather and stable stratification persist in synoptic scale. This high pressure system is thought to be enhanced by ENSO, resulting in severe dry season. The case NOBB in Table 2 excludes emission sources of biomass burning, while the case of NOEMI does not includes any emissions. In all cases listed in Table 2, full scale calculation of transport/chemistry/deposition was performed.

4. MASS TRANSPORT CHARACTERISTICS IN TROPICAL AREA AS SUGGESTED BY BACKWARD TRAJECTORY ANALYSIS

4.1 Characteristics Found in Ozone Observation at Kuala Lumpur and Watukosek

By using vertical profiles of ozone observation and backward trajectory, general feature of air mass movement over the area was studied. During the simulated period from 15 September to 4 October in 1994, vertical sounding of ozone was performed at Kuala Lumpur (KL) on 30 Sept. (Tsuruta et al. 1997) and Watukosek (WK), Indonesia on 27 Sept. (Fujiwara et al. 1998 and 1999); these are shown in Fig.1a and b (open sruares), respectively. The profiles in Fig. 1 show interesting

features that reflect transport characteristics, such as thermal stratification, in air mass over the sites. The ozone profile at KL (Fig.1a) shows rather uniform mixing ratio below about 12km, suggesting a well mixed air mass by strong deep cumulus convection. On the other hand, the ozone profile at WK (Fig.1b) has its complex structure with several pronounced local minima and maxima, indicating suppressed vertical mixing and thus a stable stratification in the air mass. This difference can be observed also in the frequency map of sub-grid scale cumulus convection (Fig.2); i.e. strong activity of cumulus convection (KL) at Sumatra and near the Malay Peninsula, and very few activities of cumulus convection (WK) over East Timor Sea and northern Australia.

Another interesting feature in Fig.1a,b is clear minimum ozone concentration at 15 km high around tropopause height. ECMWF data suggests the low ozone mixing ratios accompany local high humidity. Thus it is indicated that these air masses of the low ozone mixing ratio and high water vapor have their origin near the surface level over remote Pacific Ocean.

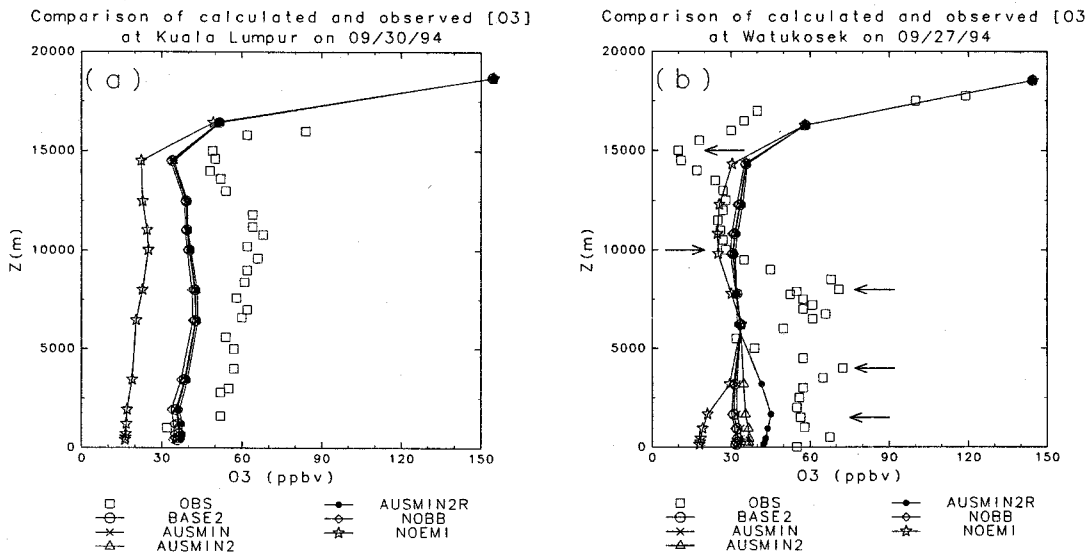

Figure 1. Observed and calculated vertical profiles of ozone: (a) Kuala Lumpur, Malaysia at 06GMT on 30 Sept 1994, (OBS: Tsuruta et al., 1997), and (b) Watukosek, Indonesia at 06GMT on 27 Sept 1994, (OBS: Fujiwara et al. 1999). See Table 2 for the simulation cases. Arrows in Fig.1b indicate characteristic local minima and maxima. Locations of Kuala Lumpur and Watukosek are shown in Fig.3.

4.2 Transport Characteristics Estimated with Backward Trajectory Calculation

To estimate origin of the air mass showing the characteristic ozone profiles at KL and WK (Fig.1a,b), 7-day backward trajectories, started at heights of 1.5, 3, 4.5, 7, 10, and 15 km high over KL and WK, were calculated (Fig.3a,b). (In the calculation vertical wind velocity in resolvable scale was used.) Figure 3a suggests at Kuala Lumpur the air mass reaching at 15 km has its origin far in Pacific Ocean and all other air masses below 10 km high came from lower troposphere over near KL area. The first finding well correlates with the low ozone and high humidity at 15 km, and the second one suggests the air mass below around 10 km near KL rather stagnates and strong cumulus convection likely occurs in it, resulting in the ozone profile in Fig.1a.

Backward trajectories of WK (Fig.3b) show completely different features from those of KL (Fig.3a). Below the height of 7 km all the trajectories show very weak vertical motion in resolvable scale and hence suggest stable stratification over the area.

From Figs.1b and 3b it can be observed that high ozone concentration below 5 km (Fig.1b) should be strongly affected by emission sources in eastern Java and northern Australia, and another ozone maximum at 7 km was formed by the transport of ozone rich air from upper layer, i.e. 9 km high, over Indian Ocean to the west of Australia. This ozone maximum of about 60-70 ppbv at 7 km may suggest long range transport from middle latitudes in southern hemisphere. Through the middle troposphere in the mid-latitudinal southern hemisphere, African biomass plumes could also migrate (e.g., Galanter et al., 2000). To check this assumption, we have done preliminary simulations by using GCTM (Global scale Chemical Transpor Model) for September in 1994, and have found that the ozone in the middle troposphere over Watukosek was transported from the middle troposphere at 20S with southerly wind induced by anticyclone which is centered at 25S and about 100E (Kitada et

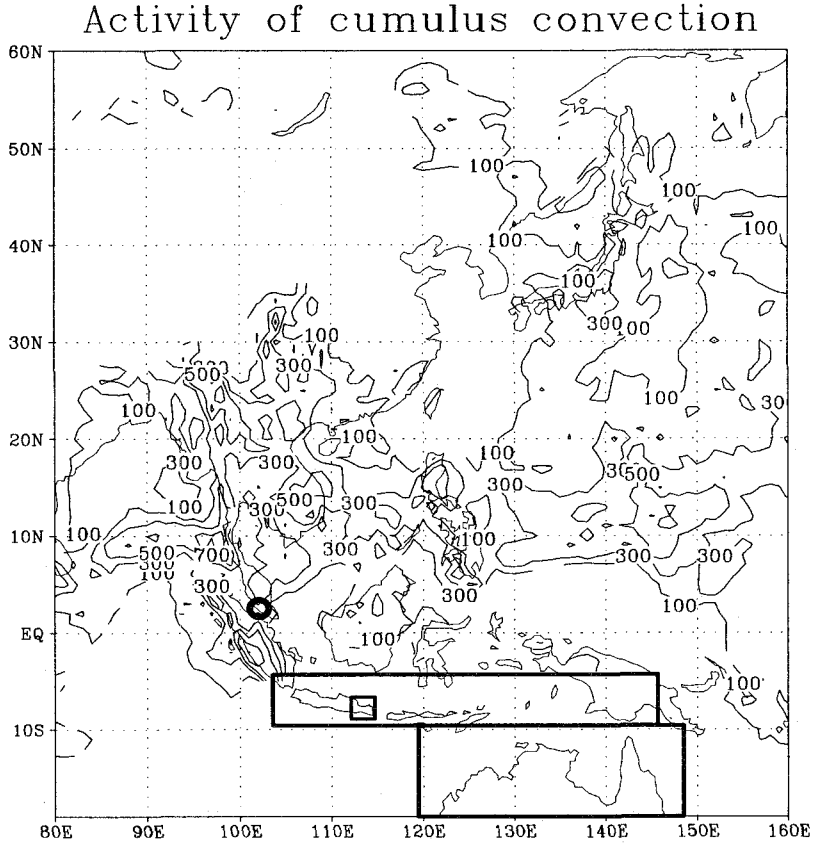

Figure 2. Spatial distribution of cumulus convection activity. Number of the application of a subgrid-scale cumulus convection scheme during three weeks from 15 Sept. to 4 Oct., 1994 is shown in the figure. To apply the scheme or not was judged every time step, i.e. 30 minutes. In the case of AUSMIN2R, biomass burining emission source in the two areas enclosed with thick solid line was given by a volume source, while AUSMIN2 uses the volume source only for northern Australia (see text and Table 2). Locations of Watukosek (□) and Kuala Lumpur (○) are also shown.

al.,2001). Furthermore extremely low ozone at 15 km (Fig.1b) may be explained by the migration of the air mass with low ozone and high humidity air, from western Pacific Ocean; the air mass was brought into the upper troposphere three days ago by the flow associated with the typhoon T26.

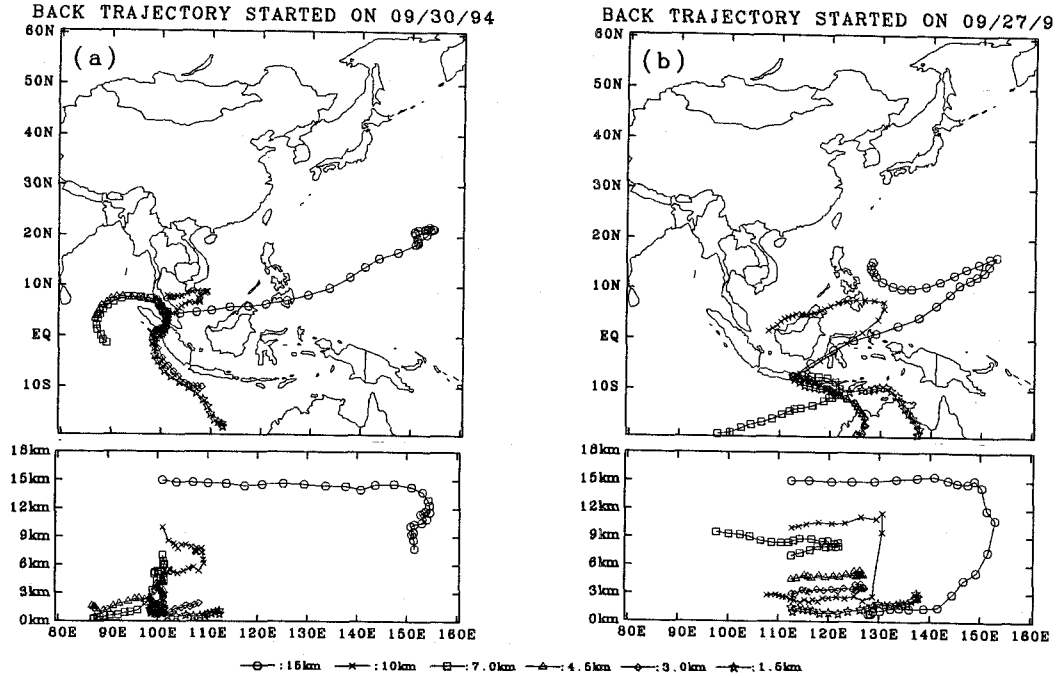

Figure 3. Seven day backward trajectory released at the altitudes of 1.5, 3, 4.5, 7, 10, and 15 km: the calculation was started from (a) Kuala Lumpur at 06GMT on 30 Sept 1994 , and (b) Watukosek at 06GMT on 27 Sept 1994. Location on the trajectory was marked every 6 hours. Wind vector in resolvable scale in 3 dimensional space was used for the calculations.

5. COMPUTED VERTICAL PROFILES OF OZONE AND CO AT KUALA LUMPUR AND WATUKOSEK, AND SURFACE OZONE AT SINGAPORE

5.1 Simulated Profiles of Ozone and CO at Kuala Lumpur, Malaysia

Computed ozone (reaction product) and CO (primary pollutant) profiles at KL and WK are shown in Figs.1 and 4 respectively. At KL (Fig.1a) all the calculated ozone profiles capture the feature of observed ozone such as rather uniform mixing ratio in the troposphere, although NOEMI predicts much smaller value compared with the other cases. The difference between AUSMIN2R (a standard case) and NOEMI of about 20 ppbv for the whole troposphere (Fig.1a) can be attributed to ozone production from its precursors which were emitted from all of the sources in the domain during 15 Sept to 30 Sept. Figure 1a (KL) shows there is a difference of about 20ppb between observation and most of the calculations. This may be due to the setting of initial ozone profile for the troposphere part in the area, judging from our test. To avoid this completely, a longer simulation in larger region,

e.g. global scale, would be required. Initial ozone profile was derived by modifing the latitude-altitude cross section estimated in Fishman and Crutzen (1978).

Figure 1a also shows that ozone profiles of AUSMIN2R and NOBB (the "no biomass fire" case) are almost same in appearance. This does not exclude, however, that biomass fire emission contributes to ozone production at KL. In fact, as shown in Fig. 4a, the biomass fire accounts for about 40 to 50% of total CO increase (i.e., derived as AUSMIN2R – NOEMI) in the middle and lower troposphere. Thus this difference in behavior of ozone and CO rather comes from nonlinearity in ozone production from its precursors, while CO is a primary pollutant directly emitted from biomass fire.

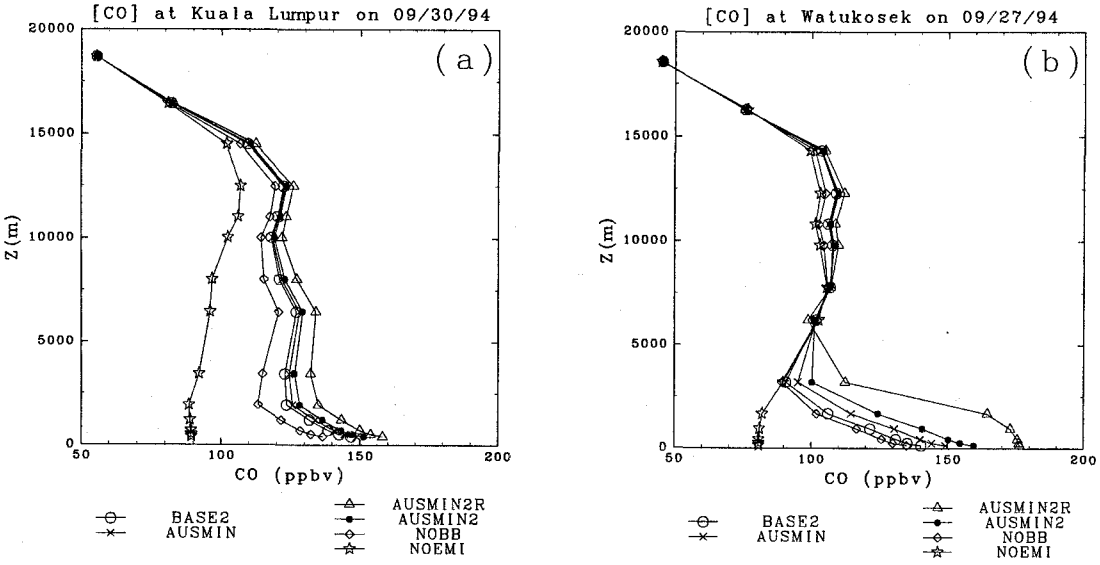

Figure 4. Same as in Fig. 1 except for CO.

5.2 Simulated Ozone at Singapore

Figure 5 similarly compares observed surface ozone at Singapore with the calculated. For the latter half of the period, the simulated ozone in AUSMIN2 well reproduced daily variation of the observation. Again, similar to Kuala Lumpur case (Fig. 1a), apparent contribution of biomass fire emissions to the ozone is small and about only 3 to 4 ppbv. It is also clearly demonstrated that without emission sources (NOEMI) the observed variation of ozone can not be explained.

5.3 Simulated Profiles of Ozone and CO at Watukosek, Indonesia

At Watukosek, in contrast to KL, the simulations were not able to reproduce some of the characteristics in the observed ozone (Fig.1b), i.e. the local maximum at 7 km in particular. As discussed in the backward trajectory (Fig.3b), the air mass at 7 km at 06GMT on 27 Sept. probably came directly from the south boundary of the domain. Hence this observed peak ozone concentration

was due to transport of ozone-rich air mass from outside of the domain. Thus the boundary conditions which could not express this inflow should be the reason why the simulations failed reproduction of peak ozone at 7 km high at Watukosek. In fact, the ozone and CO mixing ratios between 5 and 10 km in no emission case (NOEMI) are close to those in AUSMIN2R (Figs.1b and 4b) . This means ozone and CO at these heights were not produced from and by emissions in the calculation domain, but were brought in from outside of the domain. In the boundary layer and lower troposphere over Watukosek the calculations were able to qualitatively capture the characteristics in ozone profile, i.e., local maximum in ozone (Fig.1b) mixing ratio below the heights of 3-4 km.

The profiles of the calculated CO (Fig.4b) also show strong local maximum in the lower troposphere. Although there was no CO observation which allowed direct comparison with this simulation, some observed data were available for qualitative comparison; i.e., CO profiles over northern Australia and the east Timor sea were acquired in September, 1999, on the occasion of BIBLE-B campaign (Takegawa, et al., 2001). These BIBLE-B data can be considered to represent those in dry and biomass fire season over eastern Indonesia and northern Australia (see Fig. 2), which are the area dominated by a persistent anticyclone and are free from activity of cumulus convection. These CO observed profiles (Takegawa et al., 2001) show strong concentration gradient between lower (z< about 2 km high) and upper troposphere, i.e., CO with more than 200 ppbv in the boundary layer and around 80 ppbv up to 10km high above the boundary layer. The CO profile (AUSMIN2R) in Fig. 4b qualitatively reproduces these observed characteristics .

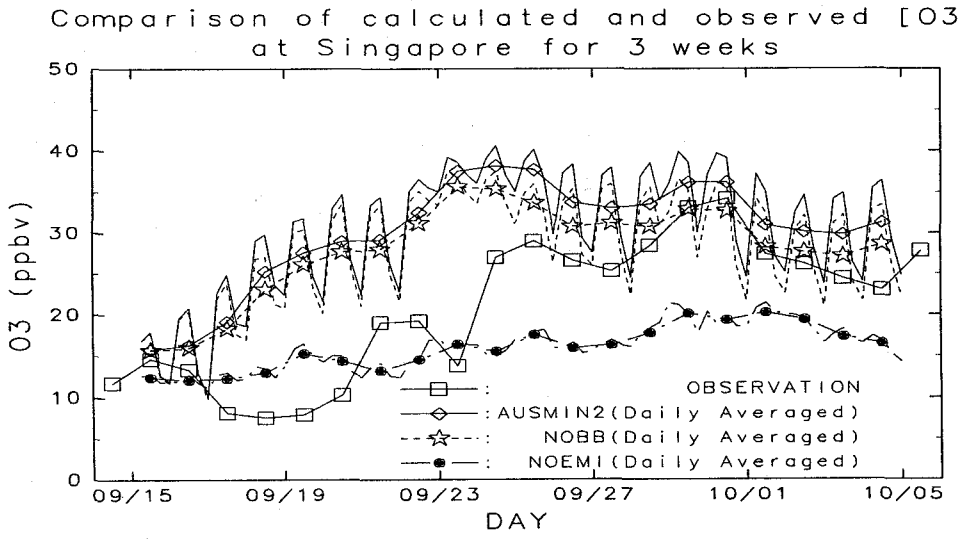

Figure 5. Temporal variation of ozone mixing ratio from 15 Sept. to 5 Oct. 1994 at Singapore: observation and calculations

5.4 Evaluation of Increase of Ozone and CO due to Biomass Fire Emissions

Effects of biomass burning on calculated concentrations can be examined by comparing NOEMI, NOBB and AUSMIN2R. Subtraction of concentration in NOEMI from those in AUSMIN2R gives increase of the species due to all of the emission souces. Similarly difference of concentration between NOBB and NOEMI shows its increase due to the sources other than biomass burning. Examination of the profiles in Figs. 1 and 4 shows effects of biomass burning on ozone and CO concentrations:

(1) At Kuala Lumpur, increase of surface ozone due to biomass fire emissions was 3-4 ppbv, and was about 15% of total ozone increase in AUSMIN2R; the total ozone increase was calculated from AUSMIN2R – NOEMI. Increase of surface CO due to biomass fire is 25 ppbv, and is about 36% of total CO increase in AUSMIN2R (see Figs. 1a and 4a). Time was 06GMT on 30 Sept.

(2) At Watukosek, increase of surface ozone due to biomass fire was 12 ppbv, and was about 48% of total ozone increase in AUSMIN2R; the total ozone increase was evaluated by subtracting ozone in NOEMI from that in AUSMIN2R. Simiarly, increase of surface CO due to biomass fire was 45 ppbv, and was 45% of total CO increase in AUSMIN2R (see Figs. 1b and 4b). Time was 06GMT on 27 Sept..

(3) At Singapore, ozone increase due to biomass fire was 3-4 ppbv (see Fig. 5).

In summary, at Kuala Lumpur and also Singapore which are located relatively far from biomass fire itself and have their own anthropogenic emissions, relative contribution of biomass fire to ozone mixing ratio is, in appearance, not so large probably due to nonlinearity of ozone production chemistry on precursors. On the other hand, CO, i.e. a primary pollutant, at KL shows rather the straight effect of biomass fire emission, suggesting about 35% of total CO increase is due to the biomass fire in Indonesia and northern Australia. Another interesting point on the profiles of CO and ozone over KL is that they are quite uniform in the troposphere. This is because of active cumulus convection over the area, and thus biomass burning emission such as CO also spreads over the whole troposphere (see Fig. 4a).

At Watukosek in Java island which is surrounded by biomass fires and is under stabley stratified condition in synoptic scale due to the dry season enhanced by ENSO, both ozone and CO in the lower troposphere are strongly influenced by the fires, e.g., about 45% of the total increases of both ozone and CO can be explained by the fires. On the vertical transport characteristics at Watukosek, in contrast to KL, the stable stratification of the atmosphere prohibits intrusion of the emissions from the local biomass fires into the upper troposphere, and thus the emissions satgnates in lower troposphere and form high concentration zone there (see Fig. 4b).

6. SPATIAL DISTRIBUTION OF OZONE MIXING RATIO AND COLUMN DENSITY AFFECTED BY BIOMASS BURNING

6.1 Horizontal Distribution of Ozone over Equatorial Southeast Asia and Northern Australia: Evaluation of the Effect of Biomass Fires

Effects of biomass burning on the spatial distribution of ozone were examined by using calculated

results. Especially the area of equatorial southeast Asia and northern Australia where severe biomass fires occured was focussed.

In the area there coexist two different climatic conditions, i.e., stable stratification with clear weather and unstable stratification with active cumulus convection. Depending on the climatic situations there can be characteristic transport processes. For example, in the dry and stably stratified area under a persistent anti-cyclone, such as northern Australia and eastern Java, initial plume rise associated with the biomass fire may be important since it could affect subsequent horizontal transport of the relreased pollutants and their life-time in the atmosphere, while, as we have already seen in Figs. 1a and 4a and discussed in 5.4, in the area of active cumulus convection such as western Sumatra, northern Borneo, and the Malay Peninsula the biomass fire emissions can be quickly transported over the depth of troposphere, and thus the pollutants may spread over larger area and affect environment in global scale (e.g., the observation by Matsueda et al. 1998). In this subsection we will examine effects of biomass fire emissions on ozone distribution at 2 km high. To see the effects at this height means to examine the effects of regional scale transport of biomass fire emissions on background concentration at receptors.

Figure 6 shows horizontal distributions of ozone related quantities at 2 km high at 06GMT on 27 Sept in a partial area (80°E-160°E, and 19°S-10°N); (a) ozone mixing ratio in AUSMIN2R, (b) increase in ozone mixing ratio by all the biomass fire emissions (AUSMIN2R - NOBB), (c) ozone increase by Australian biomass fire emissions and the volume source assumption in Java island (AUSMIN2 - BASE2), (d) effect of the elevated (volume) source assumption for biomass fire emissions over Australia, Java etc. (see Fig. 2) on the ozone increase (AUSMIN2R - AUSMIN), (e) column density, below 12 km high above the mean sea level, of the ozone increase by the biomass fire emissions (i.e. AUSMIN2R - NOBB), and (f) the same as in (e) but for by all the emission sources (i.e. AUSMIN2R - NOEMI). (see Table 2 for summary of simulation cases.)

(1) Ozone Increase due to Biomass Fire Emissions

Figure 6a shows that higher ozone concentration zone overlaps that of active emission zone extending from northern Australia to the Malay Peninsula with its maximum value of about 40-50 ppbv over eastern Sumatra, western Borneo, Java, and northern Australia. Figure 6b shows that maximum increase in ozone mixing ratio (at 2 km high) due to biomass burning source is about 8 to 10 ppbv over eastern Java, 12-14 ppbv over Australia, and about 6-8 ppbv over Sumatra and Borneo. Because of the prevailing south-easterly wind in the lower troposphere below 3 km high over Java, northern Australia, and East Timor Sea, influence of the biomass fire emissions in northern Australia and Java on ozone production spreads in the downwind area over tropical Asia south of 5°N (Fig. 6b).

(2) Ozone Increase due to Biomass Fire Emissions in northern Australia

Figure 6c shows how ozone concentartion increases at 2 km high by the addition of Australian biomass burning sources. The result suggests that Australian emissions can add ozone mixing ratio by 2 ppbv for almost whole Java and the southern Borneo, and by more than 4 ppbv for the eastern Java. In case of CO, though the relevant figure is not shown in this paper, the 5 ppbv influential line covers Sumatra and southern part of the Malay Peninsula.

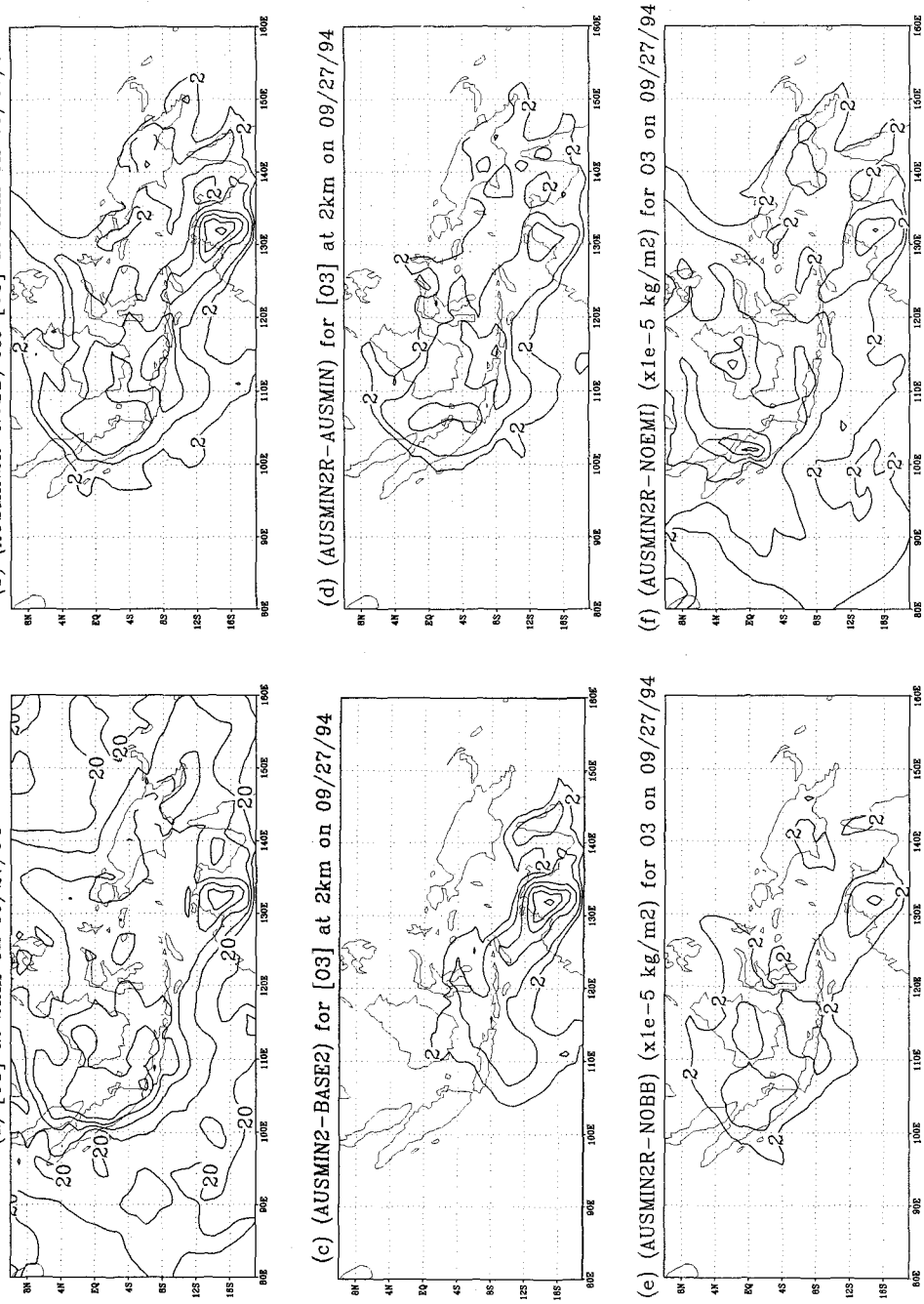

Figure 6. Calculated ozone at 2km high at 06GMT on 27 Sept 1994; (a) ozone (ppbv) in AUSMIN2R (see Table 2) , (b) ozone increase (ppbv) by all of the biomass fire emissions: (AUSMIN2R – NOBB), (c)ozone increase (ppbv) by Australian biomass fire emissions: (AUSMIN2 – BASE2), (d) ozone increase (ppbv) due to application of elevated height (volume) source for biomass fire emissions in dry area (see Fig. 2): (AUSMIN2R – AUSMIN), (e) increase in ozone column density ($x10^{-5}$ kg-ozone/m^2) below 12 km, due to all of the biomass fire emissions: (AUSMIN2R – NOBB), and (f) increase in ozone column density ($x10^{-5}$ kg-ozone/m^2) below 12 km, due to all of the emission sources: (AUSMIN2R – NOEMI). Contour interval is (a) 5 ppbv, (b)-(d) 2 ppbv, (e) $2x10^{-5}$ kg-ozone/m^2, and (f) $4x10^{-5}$ kg-ozone/m^2 ; and first contour at 20 ppbv (a), 2 ppbv (b)-(d), and $2x10^{-5}$ kg-ozone/m^2 (e) & (f).

(3) Effect of Elevated Source Assumption for Biomass Fire Emissions: Initial Plume Rise

In the stably stratified dry area in which long-standing anti-cyclone, and thus clear weather, dominates, plume rise due to heat released by biomass fire may be an important factor for the long range transport of air pollutants emitted by the fire, since a mechanism of vertical transport fast enough to carry the pollutants into lower free troposphere above ABL, such as cumulus convection, can not be expected. The fire is a subgrid scale phenomenon for the present simulations which use horizontal grids of 1° x 1° . Thus we have assumed a volume source with a height up to about 2.2 km for the fire emissions so that simulations can include some features of the plume rise. In another study we investigated this phenomenon in meso-β-scale by using MM5 with the fire heat source and 1km horizontal grid in the inner-most domain and confirmed that the vertical transport up to about 2km of biomass fire emissions is enhanced by the fire itself (Kurata and Kitada, 2000) in the "dry area" such as Java. In contrast, the released heat due to the biomass fire did not show visible effect on the vertical transport in the active cumulus convection area such as Sumatra and the northern Borneo.

Figure 6d shows increase in ozone mixing ratio at 2 km obtained as the result of the elevated source assumption for the biomass burning over northern Australia, Java etc.(see Fig. 2). The increase, for example, over eastern Java reached 6 to 8 ppbv, and by comparing with Fig. 6b, we can know that this explains almost 70-80%, in the eastern Java, of the ozone increased by the total biomass fire emissions. This means to take into account the plume rise of air mass over the biomass fire area is definitely important for long range transport over Java, East Timor Sea, and northern Australia, i.e. stably stratified area influenced by standing high pressure system. The importance of the plume rise is also supported by the fact that the case AUSMIN2R, where the concept of initial plume rise was used, reproduced a reasonable ozone profile in the lower troposphere (AUSMIN2R in Fig. 1b), though the agreement is qualitative.

Fast transport into lower free troposphere of ozone precursors such as NOx and NMHC, of course, enhanced photochemical reaction and elongated lifetime of produced ozone in stably stratified situation.

(4) Column Density of Ozone Produced by Biomass Fire Emissions and All Emissions

Figure 6e shows a snap shot, at 06GMT on 27 Sept 1994, of the ozone column density ($x10^{-5}$ kg/m^2) below 12 km high, produced by biomass burning source (AUSMIN2R – NOBB) , and Fig. 6f is the same as Fig. 6e except that effect of all of the emission sources in the domain is included (AUSMIN2R – NOEMI). Commonly used Dobson Unit can be interpreted as 1 DU = $2.14x10^{-5}$ kg/m^2. Hence from Fig.6e the column density of ozone produced by the biomass burning can be estimated as about 3 DU over eastern Java, southern Malay Peninsula, middle of Borneo etc., and about 5 DU over northern Australia.

The largest DU value in Fig. 6f appears in the area of southern Malay Peninsula and Sumatra, and its value is 11 DU. In other areas, the column density is 7 DU in northern Australia, 9 DU in the middle of Borneo, and 5 DU in western Java. Comparison beteween Figs 6e and 6f suggests that

relative contribution of biomass fire emission to the ozone column density produced by all emission sources is low at 35% in the southern Maley Peninsula, 60% in eastern Java, and high at 70% in northern Australia. Thus the biomass fire emissions influences less the ozone column density in western part of the domain because of relatively large anthropogenic emissions there.

6.2 Characteristics of Mixing Ratio and Column Density of Ozone in Whole Calculation Domain

(1) Ozone distribution Affected by Typhoon T26

Figure 7a shows ozone mixing ratio at 2 km high (AUSMIN2R) and Fig. 7b the column density of ozone, below 12 km, produced by all the emission sources (AUSMIN2R - NOEMI); both are plotted in the full calculation domain at 06GMT on 27 Sept 1994. (Figure 6e, f show partial areas of Figs. 7a,b, respectively). Figure 7a illustrates the typhoon T26 (named by Japanese Meteorological Agency) at 25°N and 135°E incorporated clean marine air into its eye region and meanwhile, it brought polluted continental air mass to the south of the typhoon over the western Pacific Ocean.
During the passage of this typhoon T26 the pollutants transport in the area near China and Japan was largely affected by it. Flow field induced by T26 advected southward the pollutants released in the northeastern- and the central-China. Thus relatively high ozone concentrations found to the north of 30°N are thought to have mostly come from stratosphere and/or area outside of northern or northeastern boundary. This is justified since simulation without any emission source (NOEMI) shows ozone field similar to Fig. 7a. The situation described here is not unusual in this season since typhoons periodically pass near the continental coast from south to north.

(2) Area of Large Ozone Column Density in Southern China

Distribution pattern in Fig. 7b is quite different from that in Fig. 7a. Since Fig. 7b represents the column density of the ozone chemically produced from both anthropogenic and natural emissions (AUSMIN2R – NOEMI) in the calculation domain, thus the ozone brought in from stratosphere or outside of the domain does not affect this column density. That is the reason why the distribution patterns in Figs. 7a and 7b are different each other. Ozone column density shown in Fig. 7b partly reflects mass distribution pattern generated by T26; i.e., the wind particularly in the lower layer induced by T26 brought ozone-precursors and the produced ozone itself into the southern China. Figure 7b shows a band of large ozone column density extending from 90°E to 120°E at about 20°N. In this area, wind is relatively weak, and cumulus convection is active (see Fig. 2). Furthermore, there are strong emission sources near the area. Thus, it is expected that large column density can appear in the area where both large emission source and strong cumulus convection activity coexist, indicating fast upward transport of pollutants by the convection enhances ozone production in upper layer and contributes to its longer lifetime.

In this sense, southern coastal China should be an interesting place since there are both strong anthropogenic emission sources and active cumulus convection. In fact, the ozone column density in Fig. 7b shows its enhancements of about 15 DU in coastal southern China. This enhancement of ozone column density agrees reasonably well with that deduced from the 15-day averaged

Meteor3/TOMS total ozone map for Sept 16-30, 1994, which is shown in Fujiwara et al. (1998); the enhancement in the Meteor3/TOMS data was about 20 DU, that was estimated by taking difference of the ozone column density between southern coastal China and the Pacific Ocean at 140° E to the east of the Philippines islands. Biomass fire was active only tropical southern hemisphere in September 1994. Thus its contribution to ozone column density in Fig. 7b was limited only over western Indonesia and northern Australia in Fig. 7b as seen in Fig. 6e.

Although Fig. 7b is a snap shot at 06GMT, 27 Sept., two weeks averaged column density from 21 Sept to 5 Oct shows the distribution similar to Fig. 7b.

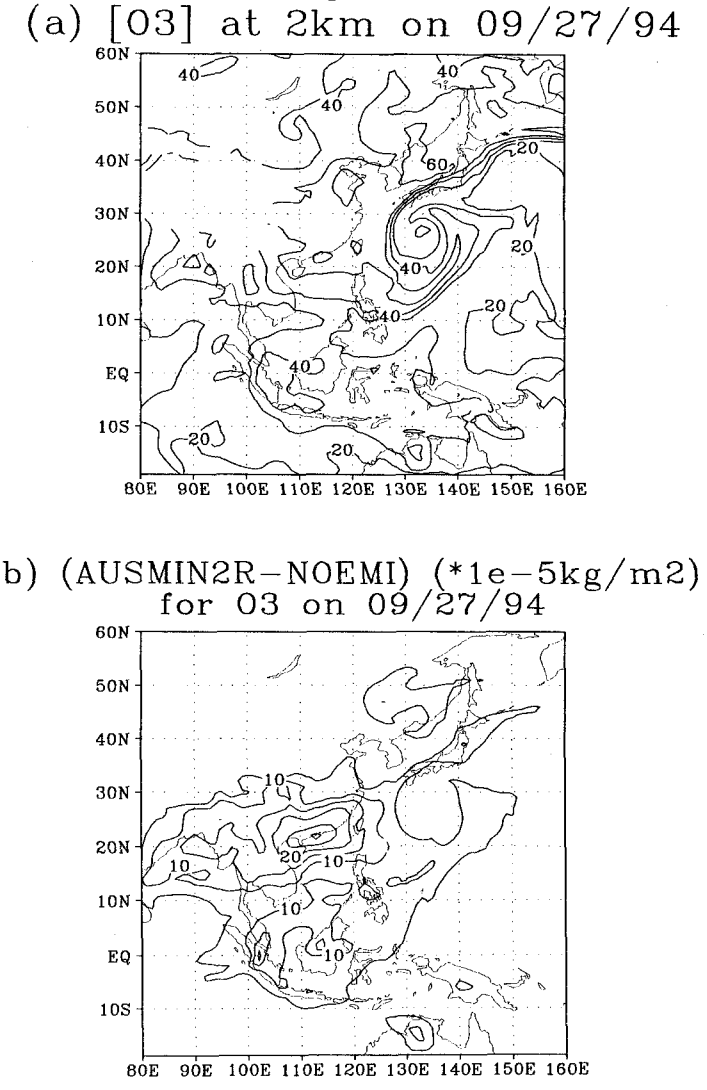

Figure 7. (a) Calculated ozone mixing ratio (ppbv) at 2 km (AUSMIN2R), and (b) ozone column density below 12 km ($x10^{-5}$ kg/m^2) produced by all the emission sources (AUSMIN2R-NOEMI) at 06GMT on 27 Sept 1994. Contour interval is (a) 10ppbv, and (b) $5x10^{-5}$ kg-ozone/m^2; first contour is (a) 20 ppb, and (b) $5x10^{-5}$ kg-ozone/m^2.

7. SUMMARY AND CONCLUSIONS

Numerical simulations of the transport/chemistry/deposition of trace chemical species were performed to evaluate the influence of biomass burning in tropical Southeast Asia on atmospheric environment and atmospheric chemistry. The following questions were tried to answer: what is the characteristic mechanism of the transport of biomass burning emissions under meteorological conditions in tropical area; how much the emissions affect concentrations in the area; and how far the emissions reach. Simulations were performed for three weeks in September and October 1994. Behavior of two chemical species, ozone as secondary pollutant and CO as primary pollutant, were focused.

Obtained results are as follows:

(1) In tropical Southeast Asia, two different meteorological situations in synoptic scale coexisted; dry and stably stratified atmosphere over Java and southern Borneo, Indonesia, and northern Australia, and wet and unstable atmosphere with active cumulus convection over Sumatra, northern Borneo, and the Malay Peninsula. In unstable and active cumulus convection area, e.g., Kuala Lumpur, Malaysia, vertical profiles of ozone and CO were rather uniform in the troposphere below 12 km (Figs. 1a and 4a), while in stably stratified area, e.g. Watukosek, Java, mass exchange between lower and upper troposphere were suppressed, and thus local biomass fire emissions were confined below 2-3 km high (Figs. 1b and 4b).

(2) Importance to include plume rise due to the biomass burning into the transport calculation was demonstrated with the simulation. The plume rise enhanced long range transport of biomass fire emissions in stably stratified area (Fig. 6d), and the inclusion of this process much improved the simulation to reproduce ozone profile at Watukosek (Fig. 4b).

(3) Increase in ozone and CO mixing ratios at surface level by biomass burning source was quantified (Figs. 1 and 4): for example, at Kuala Lumpur, ozone increased roughly by 3-4 ppbv which was about 15 % of total ozone increase by all emission sources; similarly, CO increase was 25 ppbv and was 36 % of total CO increase. At Watukosek, Java, ozone increase was 12 ppbv and was 48 % of total ozone increase; CO was increased by 45 ppbv and it was 45 % of the total CO increase.

Surface ozone at Singapore (Fig. 5) was well reproduced by the simulation. Contribution of biomass fire emissions was 3-4 ppbv, while the other sources contribute to ozone by 10-15 ppbv.

(4) The area influenced by the biomass fire in tropical Southeast Asia and northern Australia were estimated in Fig. 6b; e.g., the contour line of 4 ppbv increase in ozone at 2 km high extends over large area from 16°S to 6°N and from 100°E to 140°E, which covers almost whole eastern Indonesia such as the islands of Java, Sumatra and Borneo, the southern Malay Peninsula, and northern Australia.

(5) Tropospheric ozone column density, below 12 km, was calculated; the column density expresses that of increased ozone due to either all the emission sources or the biomass burning sources. Biomass burning sources explained 35 % of the total increase of ozone column density derived from all the emission sources, in the southern Malay Peninsula, 60% in eastern Java, and 70% in northern Australia.

(6) Calculated ozone column density (Fig. 7b) showed that in September and October of typhoon season, pollutants emitted over China gather into its southern coastal area between 10°N and

30°N, and produce and accumulate ozone in the vertical column in the troposphere. Weak wind in synoptic scale, active cumulus convection, and emission sources in central and southern coastal China and Southeast Asia may have resulted in the high ozone column density in the area. Atmospheric environment in the area should be watched because of its expected growth of energy consumption in the 21st century.

ACKNOWLEDGMENT

This work was supported in part by Grants-in-Aid for Scientific Research No. 10558083 and 1044102 from the Ministry of Education, Culture, and Science, Japan. Assistance of Ms. Yuko Nishida, former student at Toyohashi University of Technology, in doing this research is acknowledged.

REFERENCES

Cautenet, S., Poulet, D., Delon, C., Delmas, R., Grègoire, J.M., Pereira, J.M., Cherchali, S., Amram, O., and Flouzat, G., 1999, Simulation of carbon monoxide redistribution over Central Africa during biomass burning events (EXPRESSO experiment), *J. Geophys. Res.*, 104:30641-30657.

Crutzen, P.J., and Andreae, M.O., 1990, Biomass burning in the tropics: impact on atmospheric chemistry and biogeochemical cycles, *Science*, 250, 1669-1673.

EDGAR (Emission Database for Global Atmospheric Research, Version 2.0), 1997, ftp://info.rivm.nl/pub/lae/EDGARV20/; emission data for 1990.

Ferek, R.J., Reid, J.S., Hobbs, P.V., Blake, D.R., and Liousse, C., 1998, Emission factors of hydrocarbons, halocarbons, trace gases and particles from biomass burning in Brasil, *J. Geophys. Res.*, 103:32,107-32,118.

Fishman, J., and Crutzen, P.J., 1978, The origin of ozone in the troposphere, *Nature*, 274, 855-857.

Fujiwara, M., Kita, K., Kawakami, S., Ogawa, T., Komala, N., Saraspriya, S., and Suripto, A., 1999, Tropospheric ozone enhancements during the Indonesian forest fire events in 1994 and in 1997 as revealed by ground-based observation, *Geophys. Res. Let.*, 26:2417-2420.

Fujiwara, M., Kita, K., S., Ogawa, T., Komala, N., Saraspriya, S., and Suripto, A., 1998, Total ozone enhancement in September and October 1994 in Indonesia, *Proc. XVIII Quadrennial Ozone Symposium*, L'Aquila, Italy, 12-21 Sept., 1996, Vol.1, 363-366.

Galanter, M., Levy, H., II., and Carmichael, G.R., 2000, Impacts of biomass burning on tropospheric CO, NOx, and O_3, J. Geophys.Res., 105, 6633-6653.

Hao, W.M., Liu, M.H. and Crutzen, P.J., 1990, Estimates of annual and regional releases of CO_2 and other trace gases to the atmosphere from fires in the tropics, based on the FAO statistics for the period 1975-1980, in *Fire in the Tropical Biota*, Ecological Studies, Vol.84, ed. J.G. Glodammer, 440-462, Springer-Verlag.

IGBP-DIS, 1999, http://www.mtv.sai.jrc.it/projects/fire/gfp/

Kitada, T., Hara, T., Nishizawa, M., and Kurata, G., 2001, Development of Global scale Chemical Transport Model (GCTM) and its application to the transport of biomass burning emissions, *Proc. 9th Symposium on Global Environment,* JSCE, in press (in Japanese; English version of the paper is in preparation).

Kitada, T., and Nishizawa, M.., 1998, Modeling study of the long range transport of acidic pollutants over East Asia and the west Pacific Ocean –Sensitivity of acid deposition to scavenging model parameters and emission source distribution, *J. Global Environ. Eng.*, Japan Society of Civil Eng., 4:1-29.

Kitada, T., Nishizawa, M., and Kondo, Y., 1998, Long range transport of NOx, NOy, O_3, and Sox over East Asia and the western Pacific Ocean in winter season, in *Air Pollution Modelling and Its Application XII,* Plenum Pub. Co., 205-215.

Kumar, P. P., Manohar, G. K., and Kandalgaonkar, S. S., 1995, Global distribution of nitric oxide produced by lightning and its seasonal variation. *J. Geophys. Res.*, 100: 11,203-11,208.

Kurata, G., and Kitada, T., 2000, Estimation of the initial lifting height of polluted airmass due to biomass burning using meso-scale meteorological model, in *Air Pollution VII,* 157-166, WIT Press.

Lurmann, F.W., Lloyd, A.C., and Atkinson, R., 1986, A chemical mechanism for use in long-range transport/acid deposition computer modeling. *J. Geophys. Res.*, 91:10905-10936.

Matsueda, H., Inoue, H., Sawa, Y., Tsutsumi, Y., and Ishii, M., 1998, Carbon monoxide in the troposphere over the western Pacific between 1993 and 1996, *J. Geophys. Res.*, 103:19093-19110.

NASA Goddard DAAC, 1999, http://daac.gsfc.nasa.gov/

NASA LaRC, 1999, http://hyperion.gsfc.nasa.gov/AEAP/AEAP.html; emission data for 1990.

NASA Panel for Data Evaluation, 1997, *Chemical Kinetics and Photochemical Data for Use in Stratospheric Modelling.* 269p., JPL Publication 97-4.

Strand, A., and Hov, O., 1993, A two-dimensional zonally averaged transport model including convective motions and a new strategy for the numerical simulation. *J. Geophys. Res.*, 98:9023-9037.

Takegawa, N. et al., 2001, Evaluation of the effects of biomass burning on O_3 and its precursors over northern Australia in September, 1999 – Characteristics in boundary layer (z<4km)-, *Proc. 11th Symposium on Atmospheric Chemistry,* 106-108, STE Lab., Nagoya Univ., Jan. 11-12, 2001 (in Japanese).

Tsuruta, H., Yonemura, S., Peng, L.C., Fook, L.S., 1997, The increase of tropospheric ozone over Peninsular Malaysia by the 1994 forest fires in tropical east Asia, Paper presented at *International Symposium on Atmospheric Chemistry and Future Global Environment,* Int. Global Atmos. Chem., Nagoya , Japan, Nov.11-13, 1997.

Tsutsumi, Y., Sawa, Y., Makino, Y., Jensen, J.B., Gras, J.L., Ryan, B.F., Diharto S., and Harjanto, H., 1999, Aircraft measurements of ozone, Nox, CO, and aerosol

concentratios in biomass burning smoke over Indonesia and Australia in October 1997: Depleted ozone layer at low altitude over Indonesia, *Geophy. Res. Let.*, 26:595-598.

Wang, Y., Jacob, D.J., and Logan, J.A., 1998, Global simulation of tropospheric O3-NOx-hydrocarbon chemistry, I.Model formulation, J. Geophys. Res., 103, 10,713-10,726.

Ward, D.E., and Hardy, C.C., 1991, Smoke emissions from wildland fires, *Environment International*, 17:117-134.

Yienger, J. J., and Levy II, H., 1995, Empirical model of global soil-biogenic NOx emissions. *J. Geophys. Res.*, 100: 11,447-11,464.